





# A *Gaia*-Enceladus Analog in the EAGLE Simulation: Insights into the Early Evolution of the Milky Way

Lucas A. Bignone<sup>1</sup>, Amina Helmi<sup>2</sup> , and Patricia B. Tissera<sup>1</sup> 

<sup>1</sup> Departamento de Ciencias Físicas, Universidad Andres Bello, 700 Fernandez Concha, Las Condes, Santiago, Chile; [l.bignone@uandresbello.edu](mailto:l.bignone@uandresbello.edu)

<sup>2</sup> Kapteyn Astronomical Institute, University of Groningen, P.O. Box 800, 9700 AV Groningen, The Netherlands

Received 2019 July 8; revised 2019 August 19; accepted 2019 August 23; published 2019 September 17

## Abstract

We identify a simulated Milky Way analog in the EAGLE suite of cosmological hydrodynamical simulations. This galaxy not only shares similar global properties as the Milky Way, but was specifically selected because its merger history resembles that currently known for the Milky Way. In particular we find that this Milky Way analog has experienced its last significant merger (with a stellar mass ratio  $\sim 0.2$ ) at  $z \sim 1.2$ . We show that this merger affected both the dynamical properties of the stars present at the time, contributing to the formation of a thick disk, and also leading to a significant increase in the star formation rate of the host. This object is thus particularly suitable for understanding the early evolutionary history of the Milky Way. It is also an ideal candidate for re-simulation with much higher resolution, as this would allow addressing a plethora of interesting questions such as, for example, the specific distribution of dark matter near the Sun.

*Unified Astronomy Thesaurus concepts:* [Stellar kinematics \(1608\)](#); [Milky Way formation \(1053\)](#); [Galaxy mergers \(608\)](#)

## 1. Introduction

Very significant progress in our understanding of the assembly history of the Milky Way (MW) has recently been made. This was enabled by the *Gaia* mission second data release (*Gaia* Collaboration et al. 2018) in conjunction with large spectroscopic surveys such as the APO Galactic Evolution Experiment (APOGEE; Abolfathi et al. 2018), Galactic Archaeology with HERMES (GALAH; Buder et al. 2018), the RADial Velocity Experiment (RAVE; Kunder et al. 2017), and the Large Sky Area Multi-Object Fibre Spectroscopic Telescope (LAMOST; Cui et al. 2012; Zhao et al. 2012). A striking result was the discovery (Helmi et al. 2018) that a large fraction of the inner halo was made up of debris from a single galaxy named *Gaia*-Enceladus (*G-E*), which is sometimes also referred to as the *Gaia* sausage because of the signature in velocity space (Belokurov et al. 2018). This was the last significant merger that the Galaxy experienced and was estimated to have taken place  $\sim 10$  Gyr ago. It is likely that this event also had an impact on the disk present at the time, but the exact details of this process are not yet known (Gallart et al. 2019).

The key objective of this Letter is to identify, in a state-of-the-art cosmological simulation, an MW analog with a history of assembly that better resembles our current knowledge of the MW, including a merger event of similar characteristics as that found by Helmi et al. (2018). This would particularly aid in understanding its effects. Such a system would also be an excellent candidate for re-simulation (via the zoom-in technique; Katz et al. 1994; Navarro & White 1994), and allow for a more direct comparison of observations and models. Furthermore, such a re-simulation could be especially useful for studying the distribution of dark matter near the Sun (a critical input of dark matter direct detection experiments; Herzog-Arbeitman et al. 2018; Necib et al. 2018), as well as give new insights into the detailed link between the formation of various Galactic components, and possibly also other peculiarities about the MW, such as the  $\alpha$  patterns and stellar age of the

inner halo (Carollo et al. 2018; Fernández-Alvar et al. 2019) and the thick disk (Carollo et al. 2019).

In this Letter we analyze in detail a simulated galaxy extracted from the EAGLE suit (Crain et al. 2015; Schaye et al. 2015), a series of cosmological hydrodynamic simulations. This simulated galaxy has an assembly history that is similar to that currently known for the MW. We study in detail the properties of this MW analog, and in particular focus on the effects on the different galactic components present at the time of the merger with a *G-E*-like system.

## 2. *G-E* Analog Identification

The EAGLE project (see Schaye et al. 2015, for details) has been shown to produce a realistic population of galaxies reproducing a broad range of observed galaxy properties and scaling relations. Here we concentrate on the largest EAGLE simulation (Ref-L100N1504<sup>3</sup>), which has a comoving cubic volume of 100 Mpc in linear extent. The mass resolution of dark matter is  $\sim 9.7 \times 10^6 M_\odot$  and the initial mass of baryonic particles is  $\sim 1.81 \times 10^6 M_\odot$ . While the resolution of this particular simulation is lower than others available (the gravitational softening length is limited to a maximum physical size of 0.70 kpc), its large volume provides numerous MW-type galaxies with a wide range of merger histories.

As a first step in our identification of a suitable MW analog with a *G-E*-like merger, we select galaxies with virial masses in the expected range for the MW,  $M_{200} = [1, 1.5] \times 10^{12} M_\odot$  (e.g., Posti & Helmi 2019; Watkins et al. 2019). We also impose that the stellar mass inside a 30 kpc radius be greater than  $10^{10} M_\odot$  and that the current star formation rate (SFR) be in the range  $0.1\text{--}3 M_\odot \text{ yr}^{-1}$ . These simulated galaxies are then decomposed dynamically into a spheroid and a disk component (Tissera et al. 2012), where the disk is defined by star particles with circularity  $\epsilon = L_z/L_{z,\text{max}}(E) > 0.5$ , with  $L_{z,\text{max}}(E)$  being the maximum angular momentum along the main axis of

<sup>3</sup> <http://icc.dur.ac.uk/Eagle/database.php>

rotation, over all particles at a given binding energy,  $E$ . A stellar disk-to-total mass ratio criterion ( $D/T$ )  $> 0.4$ , is then imposed to ensure that our sample comprises galaxies with significant disks.

Finally, we discard galaxies that experienced a merger event with a stellar mass ratio  $> 0.15$  at any redshift  $z < 1$ . This constraint comes from the fact that the Sagittarius dwarf galaxy, with its stellar mass lower than  $5 \times 10^8 M_\odot$ , is likely the biggest merger since  $z \sim 1$  (Ibata et al. 1994). The final sample comprises 101 MW-like galaxies with diverse merger histories for  $z \geq 1$ .

A characteristic of the  $G$ -E stars is that they are on very eccentric orbits (Belokurov et al. 2018; Myeong et al. 2018). Therefore, we look for similar signs of radial anisotropy in the galaxies of our sample. To identify halo stars, we select stellar particles with  $\epsilon < 0.4$  and vertical distance from the disk plane  $|Z| > 5$  kpc (this last restriction is to diminish the possible contamination from disk or bulge stars). We then characterize the shape of the stellar halo’s velocity ellipsoid by the anisotropy parameter:  $\beta = 1 - \frac{\sigma_\theta^2 + \sigma_\phi^2}{2\sigma_r^2}$ , where  $\sigma_i$  are the velocity dispersions in spherical coordinates. We consider in the computation of  $\beta$  only stellar particles within  $5 \text{ kpc} < R < 12 \text{ kpc}$ , where  $R$  is the radial distance of the particles in the plane of the disk.

The final sample of (101) MW-like galaxies has a median  $\beta$  of 0.46. If we assume that a halo dominated by the kinematic anisotropic component has  $\beta$  more than  $2\sigma$  higher than the median (i.e.,  $\beta > 0.68$ ), five MW-like galaxies are left. We analyzed their assembly histories, searching for the accreted satellite galaxies that contributed more significantly to the anisotropic distribution and had a stellar mass ratio that is comparable to the value estimated for  $G$ -E by Helmi et al. (2018) and occurred around the estimated time by Helmi et al. (2018) and Hawkins et al. (2014). Only one of the selected halos satisfies these constraints and also has a value of  $\beta \sim 0.73$ , which is comparable to that found for the dynamical structure commonly referred to as the *Gaia* sausage (Belokurov et al. 2018; Fattahi et al. 2019). While variations in the selection criteria could result in some additional candidates, this kind of events are expected to be rare. For example, Mackereth et al. (2019) studied the origin of highly eccentric accreted stars in a smaller volume of the EAGLE simulation suit and found that only  $\sim 14\%$  of MW-mass galaxies had an accretion profiles resembling the  $G$ -E observations, using less stringent criteria.

At the time of the merger, the selected MW analog had a stellar mass  $M_* \sim 1.5 \times 10^{10} M_\odot$  and a distinct disk morphology ( $D/T \sim 0.42$ ), while the  $G$ -E analog had  $M_* \sim 3.1 \times 10^9 M_\odot$  and an irregular morphology ( $D/T \sim 0.23$ ). Table 1 lists the general properties of the MW analog at  $z = 0$  and again at  $z = 1.7$ , a time just before the  $G$ -E analog crossed its virial radius. The properties for the  $G$ -E analog are also listed in Table 1 for  $z = 1.7$ .

Figure 1 shows the dynamical properties of all stars from our MW analog at  $z = 0$  with galactocentric distances  $r_{\text{gc}} < 30$  kpc. We have separated the stars into three groups according to their circularity:  $\epsilon > 0.65$ ,  $0.4 < \epsilon < 0.65$ , and  $\epsilon < 0.4$ . These groups can be roughly considered as constituting, respectively, a “fiducial” thin disk (blue), a thick disk (orange), and a spheroid (i.e., bulge and stellar halo, green). We refer to these components as “fiducial” because the numerical resolution of the simulation prevents us from obtaining a

**Table 1**  
Properties of the MW and the  $G$ -E Analogs

Property	MW		$G$ -E ( $z = 1.7$ )	Unit
	( $z = 0$ )	( $z = 1.7$ )		
Virial mass, $M_{200}$	$1.2 \times 10^{12}$	$8.3 \times 10^{11}$	$(1.5 \times 10^{11})^a$	$M_\odot$
Virial radius, $R_{200}$	226.4	113.0	(53.2) <sup>a</sup>	kpc
Gas mass, $M_{\text{gas}}$	$6.8 \times 10^9$	$1.9 \times 10^{10}$	$3.6 \times 10^9$	$M_\odot$
Stellar mass, $M_*$	$4 \times 10^{10}$	$1.5 \times 10^{10}$	$3.1 \times 10^9$	$M_\odot$
$M_{*, \epsilon > 0.65}$	$2.2 \times 10^{10}$	$4 \times 10^9$	$4.4 \times 10^8$	$M_\odot$
$M_{*, 0.4 < \epsilon < 0.65}$	$6.4 \times 10^9$	$4.1 \times 10^9$	$5 \times 10^8$	$M_\odot$
$M_{*, \epsilon < 0.4}$	$1.3 \times 10^{10}$	$7.2 \times 10^9$	$2.1 \times 10^9$	$M_\odot$
$D/T$	0.64	0.42	0.23	

**Note.**

<sup>a</sup> Property computed at  $z = 2$ , before the start of the merger.

detailed definition of thin and thick disks. However, we can group stellar particles according to the circularity as an indicator of degree of rotational support. We plot separately the stars accreted from the  $G$ -E analog (black points). The first panel of Figure 1 shows their  $v_r$ - $v_\phi$  velocity distribution and reveals that the accreted stars have a sausage-like distribution in velocity space due to their highly elongated orbits.

The middle panel of Figure 1 shows the Toomre diagram again for all stellar particles in our MW analog. In agreement with the results reported by Koppelman et al. (2018) and Helmi et al. (2018) for halo stars near the Sun, the accreted stellar particles present slightly mean retrograde rotation. The right panel of Figure 1 shows the stellar particles binding energies versus  $L_z$ , where we see that the accreted particles belong almost completely to the  $\epsilon < 0.4$  spheroid component. As indicated by the contours in this figure, the accreted stars are less gravitationally bounded than the majority of the spheroid stars. Together with their mean retrograde motion, this makes them easy to distinguish from particles belonging to the other components. For example, a clear gap can be observed between the accreted stars and the particles with low binding energy belonging to the thick disk, which is similar to what has been observed in the MW’s solar vicinity (Helmi et al. 2018; Koppelman et al. 2018).

The qualitative similarities between the kinematics of halo stars near the Sun and the merger debris in our simulated MW analog warrants a more detailed analysis. In the following section, we thus proceed to characterize the merger and determine the effects that it had on the evolution of the different components of the final galaxy.

### 3. Results

To analyze the merger between the simulated  $G$ -E and MW galaxies, we have used data from the EAGLE snipshots, which have a temporal resolution of  $\sim 90$  Myr, which is significantly higher than that of the standard snapshots. At each timestep, we have identified the planes of rotation of the disks belonging to the main progenitor of the MW and  $G$ -E analogs. In Figure 2, we show face-on and edge-on views of different stages of the merger.

#### 3.1. Orbital Properties

We determine the orbital properties of the encounter at the time just before the satellite entered the virial radius of the main

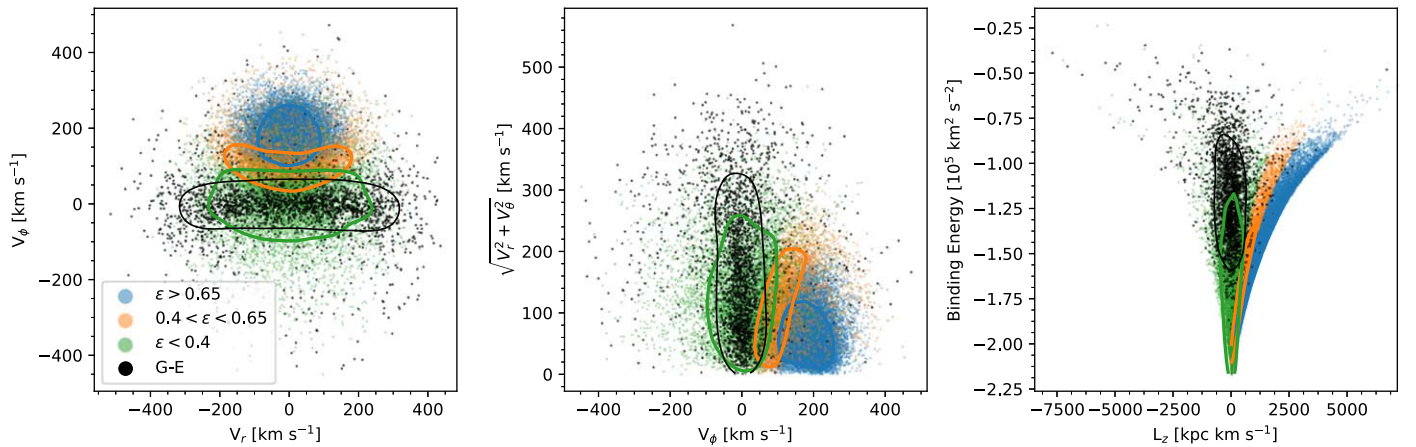


**Figure 1.** Left panel: velocity distribution of stars in spherical coordinates, radial  $v_r$  and azimuthal  $v_\phi$ , for stellar particles in an EAGLE galaxy that had a  $G-E$  type merger event. Black points represent the accreted stars from the  $G-E$  analog. Other colors represent stars in the circularity ranges displayed in the legend. Contours envelop 68% of particles in each subsample. Middle panel: Toomre diagram of stellar particles. Note that the accreted stars have slightly retrograde mean motions. Right panel: distribution of the particle binding energy vs. angular momentum, where the accreted stars have lower binding energies and slightly retrograde angular momentum, which allows for easier identification (especially for  $E > -1.25 \times 10^5 \text{ km}^2 \text{ s}^{-2}$ ). Due to the limited resolution of the simulation, we plot in the three panels the velocities of all star particles and not only those in the solar vicinity.

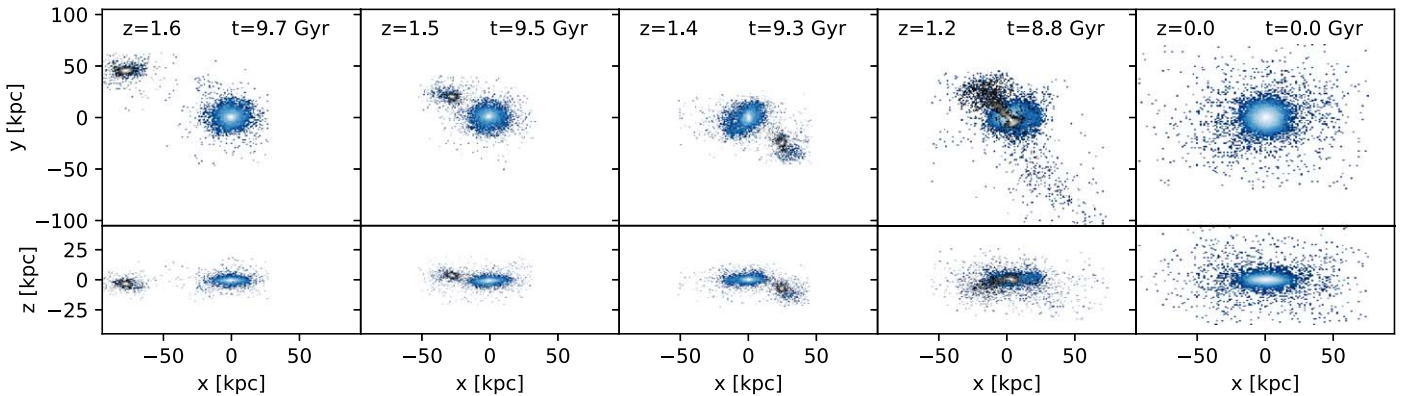


**Figure 2.** Face-on and edge-on views of the spatial distribution of stars in the MW (blue points) and  $G-E$  (black points) analogs during the merger. The reference frame has been centered on the center of potential of the host disk and has also been rotated to align the angular momentum of the main disk with the  $z$ -axis at each timestep. The last panel shows the final configuration of the MW analog at  $z = 0$ .

galaxy. The orbit of the satellite is almost coplanar with respect to the plane of the disk of the host with an inclination  $i = 6^\circ$ . The encounter is retrograde and the satellite’s spin is counter-rotating with respect to that of the main galaxy. Together, these orbital properties explain why the merger debris has retrograde orbits. Based on isolated simulations of minor mergers of (prograde rotating) disks (Villalobos & Helmi 2008), Helmi et al. (2018) found that the mean retrograde motion measured for  $G-E$  debris were best matched in the case of retrograde encounters with inclinations between  $30^\circ$  and  $60^\circ$ . Similarly, we do find that the encounter is “net” retrograde, although the inclination of our merger is lower than theirs.

In our simulation, the satellite reaches  $\sim 4.9$  kpc at closest approach in its first passage, which is then followed by a maximal separation of  $\sim 40$  kpc. The satellite has completely merged after a second passage. The dynamical effects of the merger thus lasts about 0.8 Gyr between lookback times 8.8 Gyr ( $z = 1.24$ ) and 9.6 Gyr ( $z = 1.53$ ).

### 3.2. Star Formation History

In Figure 3 we show the star formation history of the three fiducial components identified in the MW analog at  $z = 0$ . We have explicitly removed from the computation the stellar

particles accreted from the  $G-E$  analog, which we show separately (in black). Figure 3 shows an overall increase in the SFR around the time of the merger (shaded region), suggesting that the  $G-E$  analog induced star formation in the MW progenitor during their interaction. The spheroid and the fiducial thick disk also show an increase of the star formation activity during this period. Star formation in these components continues after the merger, although at a declining rate until it is quenched almost completely  $\sim 4$  Gyr ago. The effect on the fiducial thin disk, on the other hand, appears only toward the end of the merger. The gas fraction of the  $G-E$  is  $f_{\text{gas}} \sim 0.6$ , which amounts to a gas mass of  $\sim 4.5 \times 10^9 M_\odot$  out of which  $\sim 2.9 \times 10^9 M_\odot$  are converted into stars in the thin disk, representing  $\sim 13\%$  of the stellar mass of the thin disk at  $z = 0$ .  $G-E$  thus contributes a significant amount to the subsequent growth of the MW, but does not accounts for all of it.

Figure 3 shows the existence of other starbursts, particularly noticeable is that at  $z \sim 2.8$  and which is clearly evident in the spheroid component. This corresponds to another important merger with a stellar mass ratio of 0.8 that occurred around that time in this MW analog.

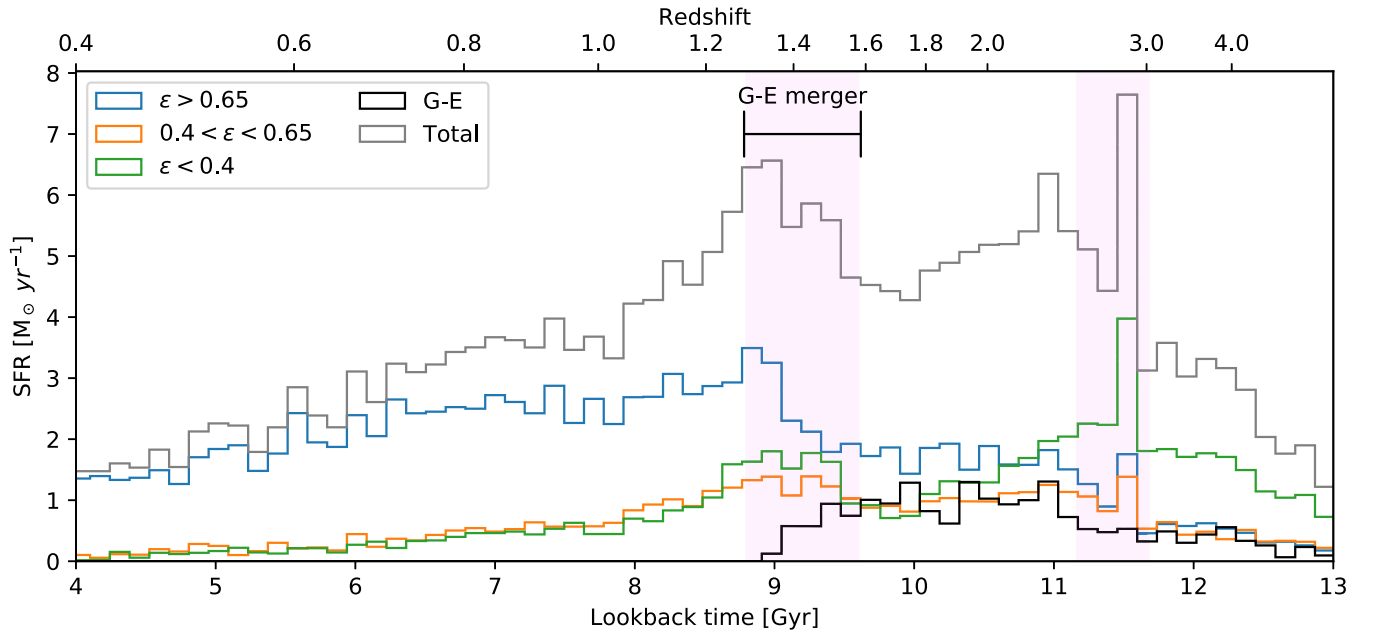


**Figure 3.** Star formation history of the host galaxy, discriminating stars in three circularity ranges at  $z = 0$  as in Figure 1. In black, we show the star formation history of stellar particles accreted from the satellite. The gray line shows the star formation history of all stellar particles. A starburst coinciding with the time of the merger (shaded interval) can be seen for all stellar particles. The shaded region on the left corresponds to a previous major merger with stellar mass ratio 0.8.

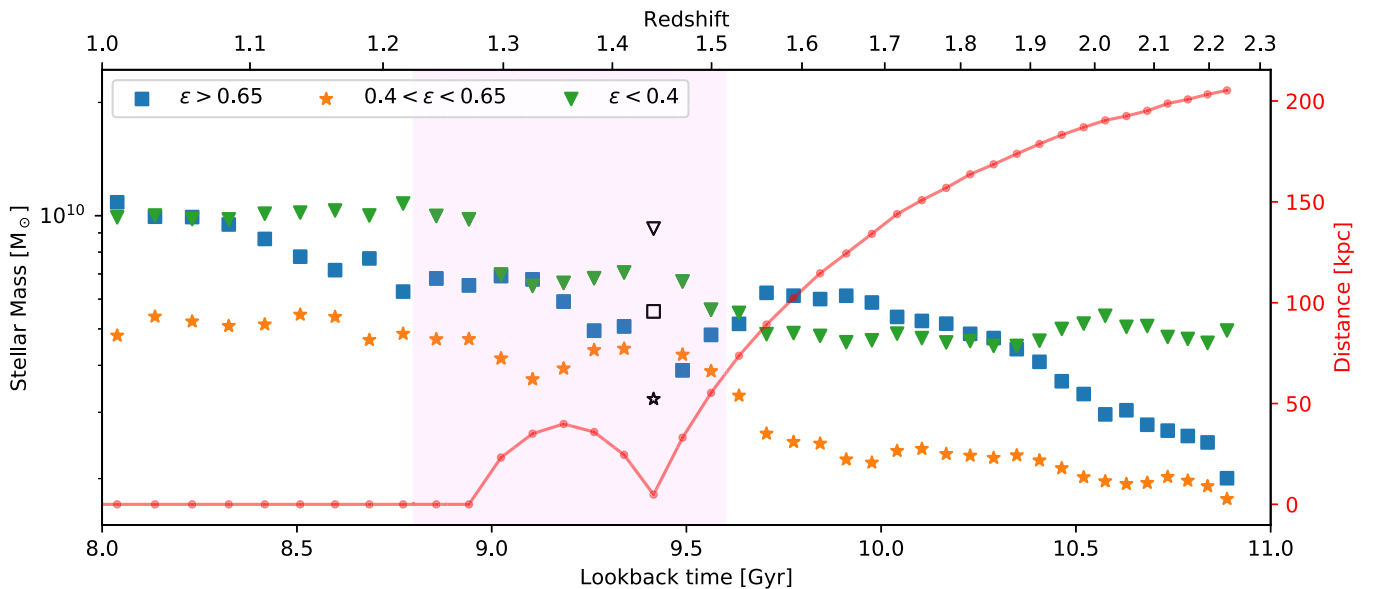


**Figure 4.** Evolution of the stellar mass content with lookback time in the host galaxy for stellar particles in three circularity ranges. The stellar mass in particles with  $\epsilon < 0.4$  presents a marked increase due to the accretion of stars from the satellite. The stellar mass with intermediate circularities ( $0.4 < \epsilon < 0.65$ ) also presents an increase just before and during the merger that can be attributed to a thickening of the disk triggered by the merger (see the text for details). The red line represents the distance between the centers of mass of the satellite and its host galaxy. The shaded region marks the lookback times between 8.8 and 9.6 Gyr, when the merger is expected to have its most significant dynamical effects. At the time of the closest approach between  $G$ -E and the MW, the assignment of particles between the host and the satellite becomes unreliable. We mark with empty symbols the points for which contamination from  $G$ -E particles is expected and exclude them from our analysis.

### 3.3. Evolution of the Structural Components

We now zoom-in around the time of the merger with the  $G$ -E analog to quantify the effect that it had on the growth of the fiducial thin disk, thick disk, and spheroid components. To do so, we identify the plane of rotation of the MW analog main progenitor at each timestep and sort the stars in each progenitor galaxy into three groups according to their circularity, in the same way that we did in Section 2 for  $z = 0$ .

In Figure 4 we show the stellar mass present in each component as function of lookback time. We also show in the

figure the galactocentric distance between the centers of mass of the MW and  $G$ -E analogs. We find that the mass of the spheroid component (green line) grows by 122% between the start and the end of the  $G$ -E merger. The mass of the fiducial thick disk (orange line) also grows considerably, by 84% during the merger. On the other hand, the fiducial thin disk (blue) starts growing more prominently during the last stage of the merger, as we had already seen in Figure 3.

Part of the growth of the spheroid component during this time interval can be directly attributed to captured stars from the satellite, as this deposits 96% of its stars in this component.

This in turn represents 19% of the  $\epsilon < 0.4$  stars at  $z = 0$ . Additional growth of this component comes from in situ star formation, most of which we can attribute to the starburst shown in Figure 3.

At disk heights  $|Z| > 5$  kpc and  $r_{\text{gc}} < 30$  kpc, 38% of the stars came from the *G-E* analog, which supports the idea that most of the MW inner halo formed from a merger that is similar to the one presented here.

The increase of stellar mass in the fiducial thick disk, however, is not due to direct accretion of stellar particles (only 3.5% of the satellite's stellar mass ends up in this component, representing 1.4% of the mass of this component at  $z = 0$ ) but is instead due to the decrease of the circularity of stars that originally belonged to the thin disk. This could be interpreted as a result of the dynamical heating induced by the merger. We also noticed that this transfer of particles between components mostly occurs just before and during the first passage of the satellite. This confirms the suggestion by Helmi et al. (2018) and Haywood et al. (2018) that the merger with *G-E* could have played a significant role in the establishment of the MW's thick disk as a distinct kinematical structure; see also Carollo et al. (2019), Gallart et al. (2019). Despite the interaction and being partially heated, the primordial thin disk is not destroyed and remains largely in place during and after the merger.

Finally, we note that less than 1% of the stars belonging originally to the *G-E* analog have  $\epsilon > 0.65$  at  $z = 0$  and they only represent 0.06% of the final fiducial thin disk, which is in agreement with previous numerical results (Tissera et al. 2012; Gómez et al. 2017).

#### 4. Discussion and Conclusions

We have analyzed a merger between a MW-like galaxy and a *G-E* analog extracted from the large cosmological box of the EAGLE simulation. We arrived at our object of study by first selecting a sample of galaxies that closely resemble the MW in terms of its present-day properties (stellar mass, virial mass, SFR,  $D/T$  ratio, and  $z < 1$  assembly history), and second by determining which galaxy presented the largest radial velocity anisotropy feature in the halo stars that could be similar to the so-called *Gaia* sausage. Curiously, we have found that the merger debris in our simulations is on a slightly retrograde orbit, as also found for *G-E*. The mean retrograde motions are in our case the result of a nearly coplanar merger between counter-rotating disks.

In the selected MW galaxy, the merger with the *G-E* analog took place between lookback times  $\sim 8.8$  Gyr and  $\sim 9.6$  Gyr and had important effects on the evolution of the host galaxy. Our analysis shows how this merger not only induced starbursts in the early disk, as expected based on previous observational (e.g., Larson & Tinsley 1978; Lambas et al. 2003) and numerical (e.g., Mihos & Hernquist 1996; Barnes 2004; Sillero et al. 2017) results, but additionally led to the formation of co-eval stellar populations that are part of the spheroid and thick disk of the MW analog at  $z = 0$ .

Furthermore, as a result of the interaction with *G-E*, stars in the early thin (and thick disk) were dynamically heated, forming the present-day thick disk. We found that most of the debris of the *G-E* merger is part of the spheroid at the present time. A large fraction of its debris in our simulation is deposited at large heights, corresponding to the stellar halo.

The simulation is therefore in agreement with a scenario where the MW experienced a significant merger early in its

history, evidence of which can be found in the present-day kinematic properties of halo stars. Furthermore, there is rough agreement between the stellar mass of the *G-E* analog ( $\sim 3.1 \times 10^9 M_{\odot}$ ) and that predicted for the event  $\sim 5 \times 10^9 M_{\odot}$  (Belokurov et al. 2018; Helmi et al. 2018; Mackereth et al. 2019; Fernández-Alvar et al. 2019; Vincenzo et al. 2019).

In terms of the timing of the event, the observed ages between 10 and 13 Gyr of *G-E* stars as inferred by isochrones (Hawkins et al. 2014; Helmi et al. 2018) is compatible with the stellar ages of the *G-E* analog, for which a median stellar age of 10.8 Gyr is found. This is also in agreement with results by Mackereth et al. (2019), who found that accreted stars in EAGLE galaxies with highly eccentric orbits could come from single mergers occurring between lookback times of 8 and 9 Gyr.

This time coincides with the simulated *G-E* merger and also with the start of the most significant growth of the thin disk. Interestingly, in our simulation *G-E* causes an increase in star formation in the MW and also contributes a significant amount of gas ( $\sim 2.9 \times 10^{10} M_{\odot}$ ) to the thin disk. This scenario resembles that proposed for the two-infall model (Spitoni et al. 2019).

Our findings show clearly that if a galaxy with global properties that are similar to the MW is also selected to have the observationally expected assembly history, it can provide insight into the early formation of the MW components. Nonetheless, we expect that a higher resolution, zoom-in simulation of this system will allow for a more detailed exploration of these processes and others, such as those related with the bulge/bar formation and the effects of the dark matter distribution.

This project has received funding from the European Union's Horizon 2020 Research and Innovation Programme under the Marie Skłodowska-Curie grant agreement No. 734374 (LACE-GAL). We acknowledge use of the Ragnar Cluster of the Laboratory for Numerical Astrophysics of Universidad Andres Bello. A.H. acknowledges financial support from NWO through a Vici personal grant. L.B. acknowledges support from CONICYT FONDECYT/POSTDOCTORADO/3180359. P.B.T. acknowledges partial support from UNAB personal grant.

#### ORCID iDs

Amina Helmi  <https://orcid.org/0000-0003-3937-7641>

Patricia B. Tissera  <https://orcid.org/0000-0001-5242-2844>

#### References

- Abolfathi, B., Aguado, D. S., Aguilar, G., et al. 2018, *ApJS*, 235, 42  
 Barnes, J. E. 2004, *MNRAS*, 350, 798  
 Belokurov, V., Erkal, D., Evans, N. W., Koposov, S. E., & Deason, A. J. 2018, *MNRAS*, 478, 611  
 Buder, S., Asplund, M., Duong, L., et al. 2018, *MNRAS*, 478, 4513  
 Carollo, D., Chiba, M., Ishigaki, M., et al. 2019, arXiv:1904.04881  
 Carollo, D., Tissera, P. B., Beers, T. C., et al. 2018, *ApJL*, 859, L7  
 Crain, R. A., Schaye, J., Bower, R. G., et al. 2015, *MNRAS*, 450, 1937  
 Cui, X.-Q., Zhao, Y.-H., Chu, Y.-Q., et al. 2012, *RAA*, 12, 1197  
 Fattahi, A., Belokurov, V., Deason, A. J., et al. 2019, *MNRAS*, 484, 4471  
 Fernández-Alvar, E., Tissera, P. B., Carigi, L., et al. 2019, *MNRAS*, 485, 1745  
*Gaia* Collaboration, Brown, A. G. A., Vallenari, A., et al. 2018, *A&A*, 616, A1  
 Gallart, C., Bernard, E. J., Brook, C. B., et al. 2019, *NatAs*, (arXiv:1901.02900)  
 Gómez, F. A., Grand, R. J. J., Monachesi, A., et al. 2017, *MNRAS*, 472, 3722  
 Hawkins, K., Jofré, P., Gilmore, G., & Masseron, T. 2014, *MNRAS*, 445, 2575

- Haywood, M., Di Matteo, P., Lehnert, M. D., et al. 2018, *ApJ*, 863, 113
- Helmi, A., Babusiaux, C., Koppelman, H. H., et al. 2018, *Natur*, 563, 85
- Herzog-Arbeitman, J., Lisanti, M., Madau, P., & Necib, L. 2018, *PhRvL*, 120, 041102
- Ibata, R. A., Gilmore, G., & Irwin, M. J. 1994, *Natur*, 370, 194
- Katz, N., Quinn, T., Bertschinger, E., & Gelb, J. M. 1994, *MNRAS*, 270, L71
- Koppelman, H., Helmi, A., & Veljanoski, J. 2018, *ApJL*, 860, L11
- Kunder, A., Kordopatis, G., Steinmetz, M., et al. 2017, *AJ*, 153, 75
- Lambas, D. G., Tissera, P. B., Alonso, M. S., & Coldwell, G. 2003, *MNRAS*, 346, 1189
- Larson, R. B., & Tinsley, B. M. 1978, *ApJ*, 219, 46
- Mackereth, J. T., Schiavon, R. P., Pfeffer, J., et al. 2019, *MNRAS*, 482, 3426
- Mihos, J. C., & Hernquist, L. 1996, *ApJ*, 464, 641
- Myeong, G. C., Evans, N. W., Belokurov, V., Sanders, J. L., & Kposov, S. E. 2018, *ApJL*, 856, L26
- Navarro, J. F., & White, S. D. M. 1994, *MNRAS*, 267, 401
- Necib, L., Lisanti, M., Garrison-Kimmel, S., et al. 2018, arXiv:1810.12301
- Posti, L., & Helmi, A. 2019, *A&A*, 621, A56
- Schaye, J., Crain, R. A., Bower, R. G., et al. 2015, *MNRAS*, 446, 521
- Sillero, E., Tissera, P. B., Lambas, D. G., & Michel-Dansac, L. 2017, *MNRAS*, 472, 4404
- Spitoni, E., Silva Aguirre, V., Matteucci, F., Calura, F., & Grisoni, V. 2019, *A&A*, 623, A60
- Tissera, P. B., White, S. D. M., & Scannapieco, C. 2012, *MNRAS*, 420, 255
- Villalobos, Á., & Helmi, A. 2008, *MNRAS*, 391, 1806
- Vincenzo, F., Spitoni, E., Calura, F., et al. 2019, *MNRAS*, 487, L47
- Watkins, L. L., van der Marel, R. P., Sohn, S. T., & Evans, N. W. 2019, *ApJ*, 873, 118
- Zhao, G., Zhao, Y.-H., Chu, Y.-Q., Jing, Y.-P., & Deng, L.-C. 2012, *RAA*, 12, 723